

# Molecular templates of spin textures on superconducting surfaces

Cristina Mier

*Materials Physics Center (UPV/EHU), 20018 Donostia-San Sebastián, Spain*

Benjamin Verlhac and Léo Garnier

*Université de Strasbourg CNRS, IPCMS, UMR 7504, F-67000 Strasbourg, France*

Roberto Robles

*Centro de Física de Materiales CFM/MPC (CSIC-UPV/EHU), 20018 Donostia-San Sebastián, Spain*

Laurent Limot

*Université de Strasbourg, CNRS, IPCMS, UMR 7504, F-67000 Strasbourg, France*

Nicolás Lorente

*Centro de Física de Materiales CFM/MPC (CSIC-UPV/EHU), 20018 Donostia-San Sebastián, Spain and  
Donostia International Physics Center (DIPC), 20018 Donostia-San Sebastián, Spain*

Deung-Jang Choi\*

*Materials Physics Center (UPV/EHU), 20018 Donostia-San Sebastián, Spain and  
Donostia International Physics Center (DIPC), 20018 Donostia-San Sebastián, Spain*

(Dated: September 26, 2021)

We create ordered islands of magnetically anisotropic nickelocene molecules on a Pb (111) substrate. By using inelastic electron tunneling spectra (IETS) and density functional theory, we characterize the magnetic response of these islands. This allows us to conclude that the islands present local and collective magnetic excitations. Furthermore, we show that nickelocene islands present complex non-collinear spin patterns on the superconducting Pb (111) surface, opening the possibility of using molecular arrays to engineer spin textures with important implications on topological superconductivity.

Topological superconductors are new states of matter that are not found in Nature. Low-dimensionality and chirality are key ingredients to create superconducting phases of different topology. A particularly interesting strategy [1–4] is to create arrays of atomic spins on a superconductor. Some inspiring results have been obtained by growing arrays of Fe atoms on Pb (111) [5, 6], and atomically placing Fe atoms on Re and Ta surfaces [7–9]. Experiments [9] and theory [10] show that topological superconductors can be obtained from islands of magnetic impurities adsorbed on an s-wave superconductor. Compelling experimental and theoretical evidence [9] show the appearance of helical Majorana states at the island boundaries in the dense-impurity regime. Furthermore, the dilute-impurity regime is also very interesting, leading to topological phases that can present numerous helical Majorana states [10].

The scanning tunneling microscope (STM) is an appropriate tool to study the above systems [11, 12]. Indeed, the STM is able to assemble atomically-precise 1D structures reaching beyond 100 spins on superconducting Re [7]. However, this technique has been unsuccessful on Pb surfaces [5, 13] mainly due to the large atomic mobility of Pb atoms on the surface. A different strategy is to use molecules that can self-assemble and create directional structures [14]. From heavy-fermion-like lattices [15, 16],

and quantum-phases on superconductors [14, 17] to functionality [18], molecules show rich spectra of physical processes and properties. Molecules can possess large spins and strong magnetic anisotropies [19] together with complex patterning. As a consequence, they can give rise to non-collinear spin textures extending the possibilities for topological superconductivity.

We report on molecular structures formed by nickelocene (Nc) molecules adsorbed on Pb (111) studied by low-temperature STM. The inset of Fig. 1 (a) shows that Nc is composed by two cyclopentadienyl rings ( $C_5H_5$ ) and a Ni atoms in between. It is a  $S = 1$  spin with sizeable hard-axis longitudinal magnetic anisotropy perpendicular to the cyclopentadienyl rings ranging from  $D = 3.4$  to  $4.0$  meV depending on the substrate [20–23]. Studies on copper surfaces [20, 21, 23, 24] show that vertical Nc molecules are intercalating with horizontal ones to form the molecular assembly. Due to the molecular magnetic anisotropy, such an assembly has the potential for producing a complex spin texture. Here, we use the sub-meV energy resolution of a superconducting-tip to investigate Nc molecular islands on Pb (111). With the help of first-principles calculations, we find that indeed the molecular arrangement within these islands imposes a non-collinear texture of interacting spins. We further show that the substrate-induced interactions lead to a

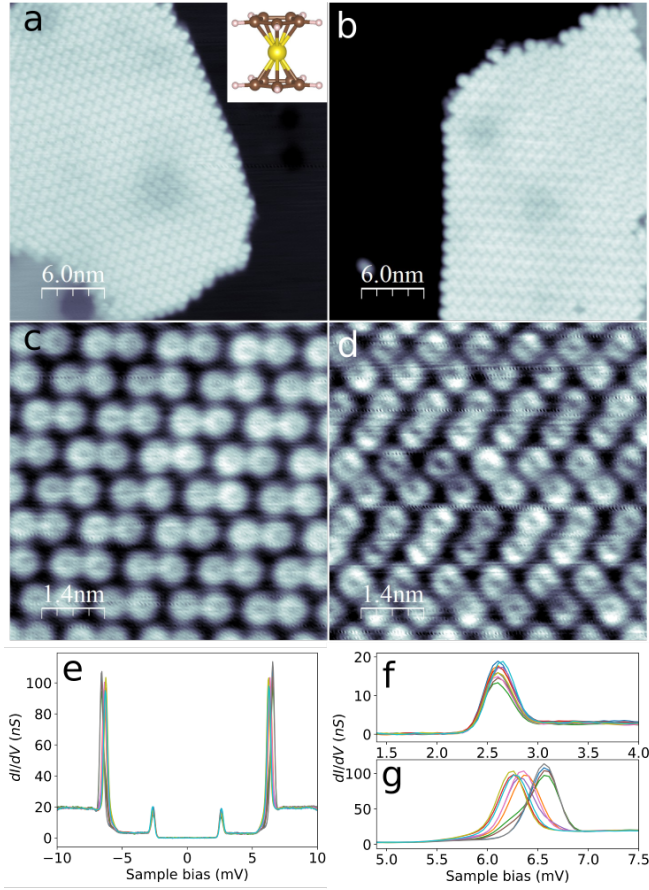


FIG. 1: (a) Constant-current image of an island of Nc on Pb (111) where the Nc dimers are aligned ( $-60$  mV,  $20$  pA,  $30 \times 30$  nm $^2$ ). Inset: the Nc molecule consists of a Ni atom (yellow) capped by C (brown) pentagons (or cyclopentadienyls) with H-saturated bonds (white), the gas-phase distance between cyclopentadienyls is  $3.6$  Å. (b) Constant-current image of Nc dimers arranged in zig-zag ( $-80$  mV,  $40$  pA,  $30 \times 30$  nm $^2$ ). (c) The *paired* arrangement of Nc dimers is evidenced at shorter tip-surface distances ( $-20$  mV,  $20$  pA,  $7.0 \times 7.0$  nm $^2$ ). (d) The zig-zag or *compact* arrangement is clearly seen at shorter tip-surface distances. (e)  $dI/dV$  obtained with a superconducting tip over several molecules at different locations. (f) The quasiparticle (QP) peak consistently appears at  $2.61 \pm 0.02$  mV, but the inelastic peak, (g), depends on the measured molecule.

dilute spin regime that is interesting for obtaining topological superconducting phases.

We deposit Nc molecules at room temperature in ultra high vacuum conditions on a Pb (111) surface kept at a temperature ranging from  $70$ - $150$  K. Figure 1 shows constant-current STM images of a representative set of molecular islands obtained on Pb (111) and at a temperature of  $2.5$  K. We find two types of arrangements after depositing the molecules. The linear arrangement of dimers, Fig. 1 (a) largely coincides with the *paired* arrangement found on Cu (100) and Cu (111) [24]. The

zig-zag configuration, Fig. 1 (b), agrees with the *compact* pattern of the previous studies [24]. This can be clearly seen in the smaller-area images of Fig. 1 (c) and (d). Different combinations of the two arrangements can take place in the same island, either repeating one pattern or the other in different domains. We perform density functional theory (DFT) studies [25] that show the two patterns share the same stabilization energy, compatible with the coexistence of both phases.

The differential conductance ( $dI/dV$ ) measured on the above systems gives interesting information on their superconducting and magnetic properties. Figure 1 (e) shows typical  $dI/dV$  measurements on molecules of the paired phase. The STM tip is coated by Pb giving a superconducting gap  $\Delta$  slightly smaller than the bulk Pb gap of  $1.35$  meV[26], due to finite-size effects [27]. As a consequence, the surface superconducting gap appears at  $\Delta_{tip} + \Delta_{substrate} \approx 2\Delta$  in the  $dI/dV$  data due to the convolution with the tip electronic structure [28–30], confirmed by the two quasiparticle (QP) peaks appearing at  $\pm 2.61 \pm 0.02$  mV in Fig. 1 (e). Zooming in into these peaks, Fig. 1 (f), shows that they are a property of the substrate and they do not depend on the molecule where the spectra are taken. However, the structure appearing about  $6.4$  mV strongly depends on the target molecule, Fig. 1 (g). These peaks correspond to the inelastic electron tunneling spectra (IETS) of the Nc magnetic excitation on a superconductor [31]. Indeed, these peaks match the excitation energy of the molecular spin from the  $S_z = 0$  ground state to the  $S_z = \pm 1$  excited states [20–23] with excitation energy  $D = 6.4 \pm 0.2 - 2.6 = 3.8 \pm 0.2$  meV shifted by  $2\Delta$  due to the presence of the tip and substrate superconducting gaps [31].

Figure 2 shows two constant-height  $dI/dV$  maps of Figure 1 (c). Panel (a) presents the spatial distribution of the  $dI/dV$  at  $V = 6.6$  and (b) at  $V = 6.0$  mV. Figure 2 (c) shows the two merged  $dI/dV$  maps reproducing the dimer pattern of Fig. 1 (c). Both maps, Fig. 2 (a) and (b), show a quasi-periodic pattern involving three dimers, instead of the single-dimer periodic structure of Fig. 1 (c). In order to understand these spatial IETS peak patterns, Fig. 2 (a) and (b), the location of the dimers on the substrate needs to be found. To do this, we perform STM images on the edge of the compact island at different tunneling currents to obtain atomic resolution of the Pb (111) substrate [25]. From these data, the unit cell of Fig. 2 (d) emerges. As in previous studies [23, 24, 32] a combination of vertical (with the molecular axis perpendicular to the surface) and horizontal (parallel to the surface) Nc has to be considered. The new pattern consists of two vertical molecules and two horizontal molecules. The experimental angle of the structure is  $50^\circ \pm 4^\circ$ , in good agreement with the angle of  $53.5^\circ$  we find by using DFT to optimize a structure based on 3 vertical and 3 horizontal dimers [25].

We further compute different molecular-layer ener-

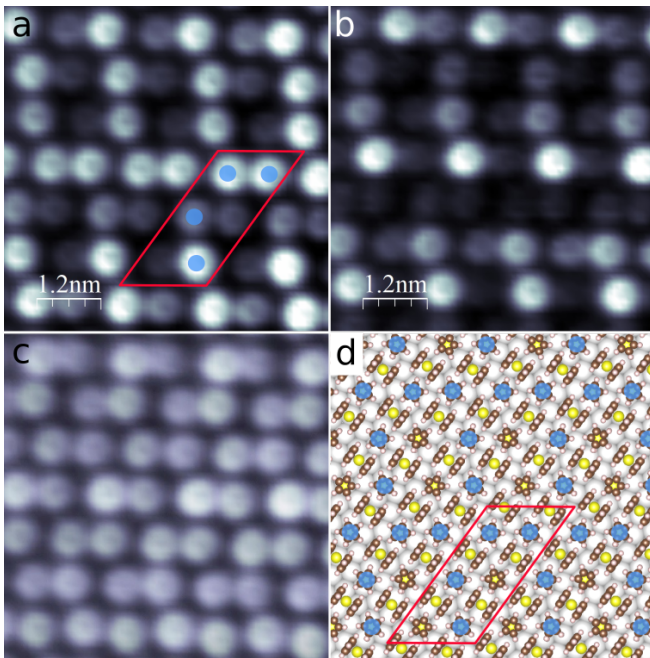


FIG. 2: (a) Constant-height  $dI/dV$  map taken at 6.6 mV, and (b) at 6.0 mV over the *paired* phase, Fig. 1 (c). (c) The two maps are merged into one single map, showing the same dimer structure as the constant-current image and hence their complementarity. (d) Atomic structure of the unit cell for the aligned-dimer phase. The maps in (a) and (b) point at a unit cell formed by three vertical and three horizontal dimers aligned within an angle of  $50^\circ$  with the  $[\bar{1}01]$  direction of the Pb (111) surface. The Nc molecules with the smallest computed MAE (FCC and bridge sites) are marked by a circle on the corresponding vertical molecule. The emerging pattern perfectly matches the  $dI/dV$  map at 6.6 mV in (a). The complementary pattern is also obtained and it is due to the molecules on the remaining top sites that present a lower MAE than on the FCC and bridge sites.

gies by shifting the molecular structure over the surface. All the computed structures are basically equivalent, with the larger energy difference being only 20 meV per molecule. This feeble dependence on the actual adsorption sites show the small corrugation of the substrate-molecule interaction. As a consequence, the molecular structure presents some degree of incommensurability [33] that translates in the quasi-periodicity of the IETS pattern Fig. 2 (a) and (b). The two types of molecules (vertical and horizontal) lead to different interaction with the substrate. The horizontal molecules are weakly interacting via vdW forces and their computed adsorption energy is 0.5 eV/molecule. However, the vertical molecules do present hybridization between their frontier  $\pi$  orbitals and the  $sp$ -electronic structure of the Pb (111) surface with 0.7 eV of adsorption energy per molecule.

Extra information of the magnetic interactions at play

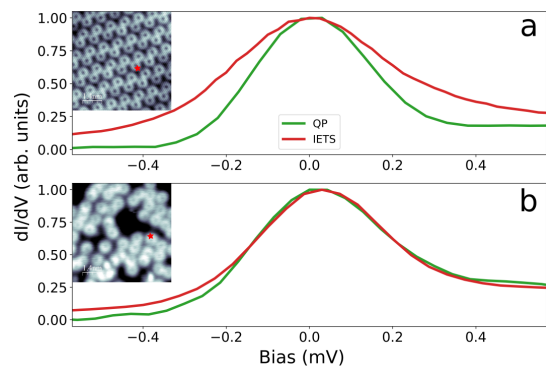


FIG. 3: (a) Lineshape of the IETS peak superimposed on the QP peak by shifting their respective bias origins and rescaling the peaks, for (a) a molecule in an order island (inset shows the tip location) and (b) for a molecule with few neighbors in a disordered island (see inset). Molecules with large regular neighbor coordination show an extra source of broadening for the IETS peak.

can be obtained from the IETS lineshape. Figure 3 superimposes the  $dI/dV$  lineshape of the IETS on the QP peaks. In the case of (a), the  $dI/dV$  spectra were obtained on a highly-coordinated molecule in a ordered island shown in the inset. The case of (b) corresponds to a lowly-coordinated molecule in a disordered island, see inset. These figures hint to an extra source of broadening for the IETS peak in the ordered case.

In order to explain the magnetic IETS data, we perform non-collinear DFT calculations with spin-orbit coupling. We obtain a clear relation between the magnetic anisotropy energy (MAE) of a single molecule and its adsorption site [25]. The unit cell contains an admixture of FCC, top and bridge adsorption sites. The single-molecule MAE calculations yield a shift of  $-0.47$  meV for molecules sitting on FCC and bridge sites with respect to the gas-phase molecule, matching the pattern at larger bias. Figure 2 (a) is in good agreement with (d). On the top site, the shift is  $-0.67$  meV, explaining the experimental pattern at lower bias. Albeit small, the MAE dependence on adsorption site can be traced back to the hybridization of vertical molecules with the substrate, see the supplementary information [25]. Figure 4 (a) sketches the ground-state spin texture of the resulting molecular adlayer.

We also evaluated the intermolecular magnetic interactions using different non-collinear spin configurations, minimizing the energy and fitting a generalized Heisenberg exchange tensor [12, 25, 34, 35]. The interactions along the vertical dimer rows, red arrows in Fig. 4 (a), are ferromagnetic with isotropic exchange values of 1.26 meV intradimer and 1.59 meV interdimer along the row. The horizontal dimer rows are antiferromagnetic with isotropic exchange couplings of 1.61 meV intradimer and



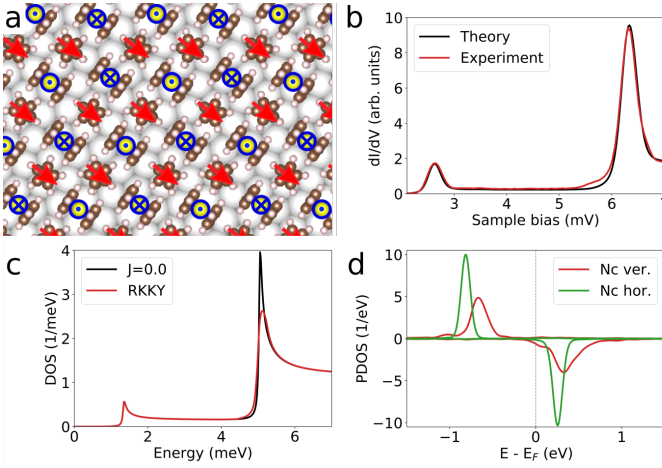


FIG. 4: (a) Spin texture on the Nc *paired* pattern. The vertical-molecular rows present ferromagnetic coupling (surface in-plane red arrows), while the horizontal molecules have antiferromagnetic coupling (blue crosses and points representing inward/outward arrows respectively). Due to the large axial magnetic anisotropy, the spins are constrained to the plane perpendicular to the molecular axis. (b) Simulated  $dI/dV$  (black) compared with the experimental one (red) using Bloch’s spinwave theory and a molecule–molecule 3-D RKKY exchange coupling. (c) The red line is the electronic DOS used in the  $dI/dV$  of (b) and the black line is the DOS for a zero intermolecular exchange coupling ( $J = 0.0$ ). The spinwaves shift the inelastic peak to higher energies and present a broadened DOS. (d) DOS projected on the Nc  $\pi$  frontier orbitals. The red curve corresponds to vertical molecules, that hybridize with the substrate shifting to higher energies the molecular orbitals and broadening them. The green curve is the DOS for the horizontal molecules displaying a weak interaction with the substrate.

0.87 meV interdimer. Moreover, the interaction between vertical and horizontal molecules amount to a small exchange coupling of 0.3 meV, while the ferromagnetic interaction between vertical rows is a bigger exchange coupling of 0.8 meV. These facts draw a picture of long-range interactions that facilitate the collective response of the molecular adlayer to external perturbations.

The IETS lineshape is then a combination of local molecular spin excitations and delocalized spinwave excitations. Their combination can be accounted for by using Bloch spinwave theory [36] and we evaluate the differential conductance as the convolution of BCS densities of states in the presence of excitations [25]. Figure 4 (b) shows the calculation of the  $dI/dV$  for an isotropic 3-D RKKY exchange coupling and a local anisotropy  $D = 3.7$  meV. The experimental features are correctly described under the above assumptions, particularly the extra broadening of the IETS peak compared to the QP one of Fig.3 (a). The effect of the spinwaves is to broaden and shift the spectra of the local excitation, Fig. 4 (c).

A complex non-collinear spin texture like the one

above, on a superconducting surface is prone to display Majorana states [2, 3, 10]. With this aim, we study the presence of in-gap Yu-Shiba-Rusinov states [37] by first evaluating the electron-molecule exchange interaction and next the value of the in-gap eigenenergy. Figure 4 (d) shows the projected density of states (DOS) of a Nc molecule on a bridge site. The symmetrically occupied/empty states about the Fermi energy correspond to the majority/minority spins of the Nc  $\pi$  frontier orbitals. From the orbital splitting we can estimate the molecular charging energy to be  $U \approx 0.9$  eV. The peaks present a broadening  $\Gamma \approx 0.2$  eV. Using the Schrieffer-Wolf transformation [36] we obtain that  $\pi J_K \rho \approx 0.44$ , where  $J_K$  is the Kondo coupling and  $\rho$  is the normal-state DOS at the Fermi energy. The Yu-Shiba-Rusinov state energy for this symmetrical case is  $\epsilon_0 = \Delta(1 - \alpha^2)/(1 + \alpha^2) \approx 0.8\Delta$ , where  $\alpha = \pi J_K \rho S/2$ , with  $S = 1$  for Nc. This type of system closely resembles the Shiba-chain limit studied by Pientka and co-workers [2, 3] and the dilute limit of 2D islands studied by Li *et al.* [10], which can show topological phases characterized by large Chern numbers and thus have several helical Majorana modes.

A careful inspection of the superconducting gap around the edge of the Nc islands permits us to conclude that there is no such state and hence no topological phase [2, 3, 10]. Probably due to the closeness of the in-gap states to the QP peaks. Compressing the molecular layer [38, 39], functionalizing the molecules or enhancing the reactivity of the superconductor surface are strategies that can approach in-gap state towards zero energy and drive the Nc/Pb (111) system into the topological phase.

In summary, Nc molecules self-assemble aligning their molecular axis in two different directions, creating molecular islands with non-collinear spin structures. The role of the substrate is crucial in creating the spin texture that translates into geometrical patterns of the IETS signal as well as a broadened lineshape due to the presence of local spin excitations and non-local spinwaves. The lack of direct interaction between vertical molecules makes of this system a first example of dilute non-collinear spin impurities that can create topological superconductors characterized by large Chern numbers. We believe that topological phases can be made accessible by small modifications of the molecular islands.

These results show that molecular layers can create rich spin textures through the interplay of different interactions. This has important implications on superconductors because these spin textures can create domains of different topological character, leading to new material design.

Financial support from the Spanish MICINN (project RTI2018-097895-B-C44), the European H2020 FET open project MeMo (grant no. 766864) and the French Agence Nationale de la Recherche (grants no. ANR-13-BS10-0016, ANR-11-LABX-0058 NIE and ANR-10-

LABX-0026 CSC) are gratefully acknowledged.

### Supplemental material: Molecular templates of spin textures on superconducting surfaces

#### Density functional theory calculations

Calculations have been performed in the framework of density functional theory as implemented in the VASP code [40] using the projected augmented-wave (PAW) method [41]. Wave functions have been expanded using a plane wave basis set with an energy cut-off of 400 eV. We used PBE as GGA-functional [42]. This functional was completed with dispersion corrections introduced through the D3-BJ scheme [43, 44]. The Pb (111) surface was simulated using a 5 layers slab with a vacuum region of 16 Å. The three upper layers plus the molecules were relaxed until forces were smaller than 0.02 eV/Å. The calculations of isolated molecules and dimers were performed for a  $6 \times 4\sqrt{3}$  Pb (111) cell, using a k-point sampling of  $3 \times 3 \times 1$ .

STM images have been simulated within the Tersoff and Hamann approximation [45] using the method described by Bocquet et al. [46] as implemented in STMpw [47].

#### Determination of the molecular adlayer

Atomic resolution on Pb (111) was obtained approaching the tip to the substrate. Figure 5 (a) shows atomic resolution close to a Nc island. From the determination of the surface main direction, we can determine the orientation of the island. We obtained an angle of  $47-48^\circ$  between the dimerization direction of the Nc layer and the  $[\bar{1}01]$  direction of the (111) Pb crystal. Figure 5 (c) and (d) correspond to constant current images of the molecular layer at  $-20$  mV and  $-5$  mV respectively. At a bias of  $-20$  mV the ring of the molecule is most visible, at  $-5$  mV a small corrugation can be observed at the expected location of the horizontal Nc. The blue hour-glass (circle) indicate the position of the horizontal (vertical) molecules. The unit cell shown on Fig. 2 from the main text is also depicted here in red.

The structure of Fig. 2 of the main text for the linear arrangement was obtained looking for a commensurate cell fulfilling (i) the above orientation with respect to the surface, (ii) the dimer structure observed in the topographic images, and (iii) the supercell emerging from the dI/dV maps showing three dimers. Taking into account all these conditions and patterns found in previous works [24], a 12-molecule supercell was proposed and optimized. The supercell is determined by vectors  $(5 \ -1)$  and  $(3 \ 7)$  which form an angle of  $53.9^\circ$ , in good agreement with the  $50 \pm 4^\circ$  experimental angle. The angle with the  $[\bar{1}01]$

direction of the surface is  $48.7^\circ$ , also in good agreement with the experimental data.

The molecular adlayer was consequently shifted with respect to the surface, so as the first molecule occupied a top site, then HCP and FCC hollow sites, and a bridge site, originating 4 different configurations for the surface structure. The 4 structures were relaxed and their final energies were within 20 meV/molecule, showing the small corrugation of the molecule-surface potential energy surface.

We performed extra calculations of a single molecule and a single dimer supported on the Pb (111) surface. From these calculations we can glean more information about the interactions of the molecules with the surface. The adsorption energy is defined as the energy needed to desorb the molecule. This can be obtained by subtracting the energy of the molecule on the surface fully-relaxed system from the free molecule energy plus the free-surface energy (fully relaxed). The resulting positive number is the energy needed to go from the adsorbed system to the desorbed one assuming there are no barriers in-between these two asymptotic configurations.

The adsorption energy of a single vertical molecule is 0.668 eV. From here the vdW contribution is 0.435 eV leaving a chemical hybridization of 0.233 eV. The dimer adsorbs with an energy of 0.682 eV/molecule, the extra binding energy comes from the vdW interaction between the two molecules. The adlayer shows an even larger adsorption energy per molecule (0.939 eV/molecule) due to the extra stabilization furnished by the intermolecular interactions. Indeed the cohesion energy of the adlayer in the gas phase is 0.438 eV per molecule. As expected, it is more difficult to desorb a single molecule from the molecular adlayer on the surface than a single molecule on the surface.

Additional information can be extracted from the projected density of states (PDOS) of the single molecules on the surface (Fig. 6). The comparison between the PDOS of vertical and horizontal molecules shows the higher degree of hybridization of the vertical molecules, where the  $\pi$  orbitals are pointing towards the surface. Among the vertical molecules the top case presents an upshift of around 100 meV with respect to the other cases.

#### Linear and zig-zag arrangements

As explained in the main text, we find two arrangements after deposition of the molecules: linear and zig-zag. We have studied both of them in the unsupported case. Without considering the surface the linear configuration can be described using a unit cell containing two vertical and two horizontal molecules, as can be seen in Fig.7a. In order to describe the zig-zag configuration the unit cell has to be doubled to accommodate four vertical and four horizontal molecules (Fig.7b). The corre-

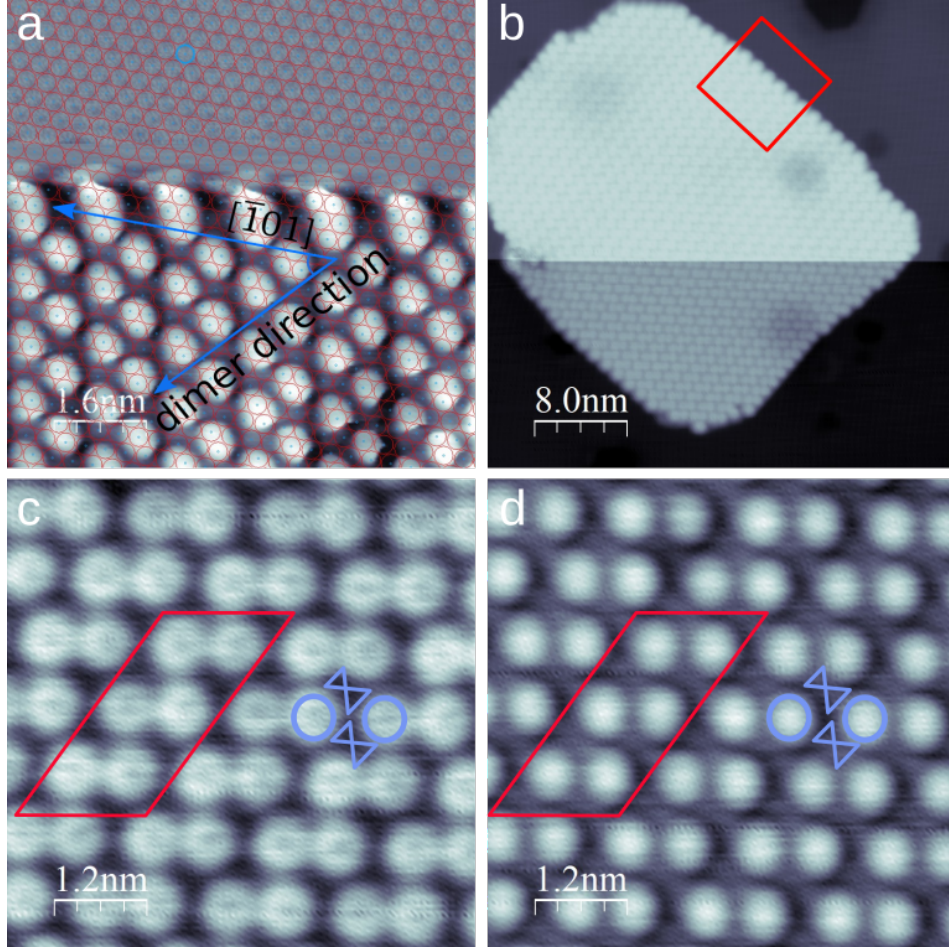


FIG. 5: (a) STM image with surface atomic resolution in the upper part of the image, the red circles indicate the hexagonal lattice on the Pb (111) surface. (b) Lower-current image, permitting to visualize the full Nc island. The red square marks the area of image (a). (c) Zoomed area of the molecular layer at 20 pA and  $-20$  mV. The blue schemes depict two vertical molecules (circles) and two horizontal ones (hour-glass schemes). (d) Same as (c) but with a bias of  $-5$  mV.

sponding simulated STM images in Fig.7d and Fig.7e are in good agreement with the experimental images, taking into account that we are not considering the surface here. For comparison we have calculated the STM image of the supported case in Fig.7f. Energetically linear and zig-zag arrangements are close. We obtain a binding energy of 0.438 eV per molecule for the linear case and 0.425 eV for the zig-zag one. Although the calculations have been done in the gas-phase, the mainly vdW nature of the interaction with the surface and the small corrugation of the molecule-surface potential energy surface shown before make us believe that both arrangements will be energetically close also on the surface, in agreement with its coexistence in the experiment.

#### Single-molecule magnetic anisotropy

Table I summarizes the main results concerning the calculations of magnetic anisotropy for single molecules.

The anisotropy is calculated like in Ref. [20] and reproduces the overall values. The energy of the molecule is computed for a non-collinear spin configuration with spin-orbit coupling. The energy is minimized self-consistently for two different directions of the spin, one along the molecular axis and the other one perpendicular to it. Since the molecular spin is  $S = 1$ , the energy difference between both configurations readily gives the value of  $D$ , as for example used in Eq. (2). The values are about a factor of two smaller than the experimental ones, as it is common of DFT calculations with spin-orbit coupling [48–50]. In this work, we are interested in the trend of the MAE with adsorption site, that is more reliable than MAE absolute numbers.

Table I shows that the MAE strongly depends on the adsorption site. This explains the distribution we find of the  $dI/dV$  peaks, because they correlate the geometrical position of the molecule with the value of its MAE.

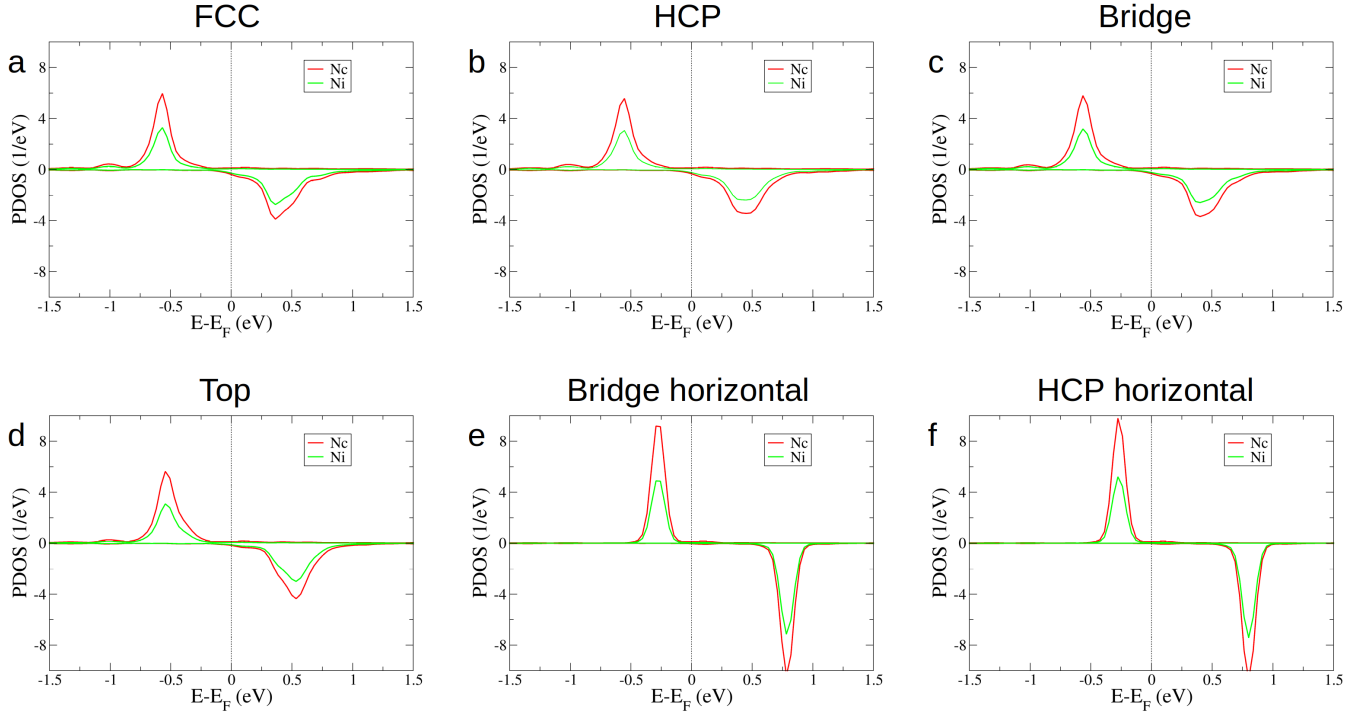


FIG. 6: Projected densities of states (PDOS) of a single molecule on the surface at different adsorption sites. (a-d) shows the PDOS at vertical molecules, while (e-f) represents the PDOS at horizontal ones. A Gaussian broadening with  $\sigma = 50$  meV has been applied.

Vertical molecule			
Site	magnetic moment ( $\mu_B$ )	Ads. energy (eV)	D (meV)
Free	2.0	—	1.77
FCC	1.77	0.67	1.30
HCP	1.77	0.65	1.50
Bridge	1.78	0.65	1.30
Top	1.83	0.61	1.10
Horizontal molecule			
Bridge	1.95	0.54	-1.72
HCP	1.95	0.52	-1.71

TABLE I: Calculated single-molecule adsorption and anisotropy energies together with the molecular magnetic moment for single Nc molecules on Pb (111).

### Exchange-coupling evaluation

After minimizing the energy of different spin configurations with spin-orbit coupling, we find that vertical dimers are ferromagnetically coupled in the supercell. Horizontal molecules are antiferromagnetically coupled. The spins are at about  $14^\circ$  off the vertical dimer rows and in-plane, while the horizontal dimers present out of plane spins. No degree of chirality is discernible from these calculations.

The exchange coupling is obtained by fitting a gener-

alized Heisenberg interaction of the form:

$$\hat{H} = \hat{H}_0 + \sum_{i,j} \vec{S}_i \cdot J_{i,j} \cdot \vec{S}_j. \quad (1)$$

Here,  $J_{i,j}$  is a tensor on the spatial coordinates of the spins  $\vec{S}_i$  and  $\vec{S}_j$ . In the absence of spin-orbit interaction the SU(2) symmetry is preserved and the tensor becomes a scalar yielding the usual Heisenberg interaction. The spin-orbit coupling breaks the spin symmetry and gives rise to anisotropic terms. Usually, the tensor is then divided in three terms [12, 34], an isotropic one that is the Heisenberg exchange ( $\text{tr}(J_{i,j})/3$ ) and the anisotropic one that is the tensor without the trace term. The anisotropic tensor is further divided in antisymmetric and symmetric



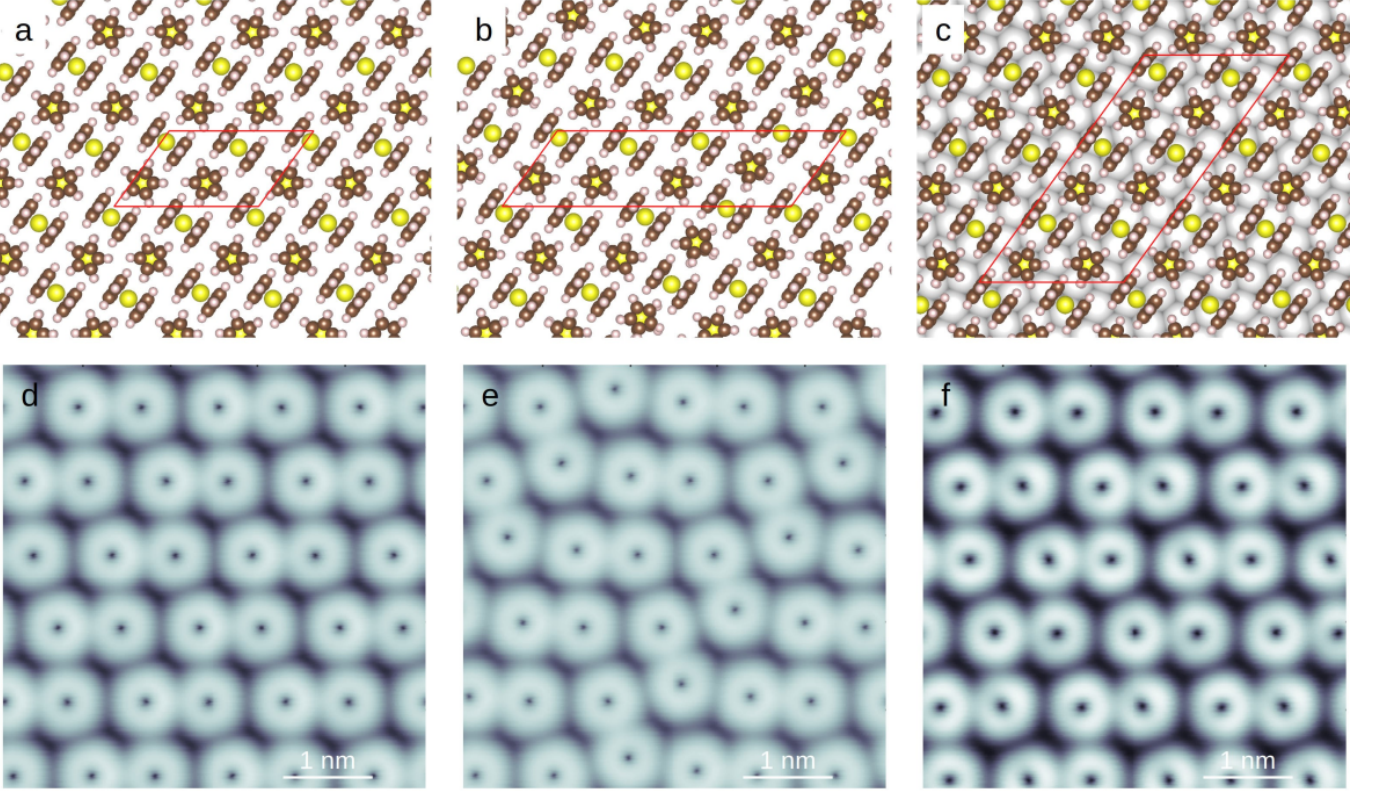


FIG. 7: Unsupported structure of the linear (a) and zig-zag (b) arrangements of dimers. The corresponding simulated STM images are shown in (d) and (e), respectively. (c) shows the linear arrangement supported on Pb (111) with the unit cell derived from the dI/dV maps, with the corresponding simulated STM image shown in (f).

tensors because the antisymmetric one exactly yields the Dzialoshinskii-Moriya interaction.

On Pb surfaces the spin-orbit coupling cannot be neglected. Even if the isotropic Heisenberg interaction is the only one to be considered, the results greatly vary with and without spin-orbit coupling.

To obtain the isotropic Heisenberg interaction, only two collinear configurations are needed per interaction. This permits us to simplify the calculations. For the case of a single dimer, we further use two chiral configurations to obtain the anisotropic contributions to the tensor because the local longitudinal anisotropy of the Nc molecule constrains the spin to the molecular plane. The exchange tensor of Eq. (1) is only a  $2 \times 2$  matrix in this case. The diagonal components are determined from the collinear calculations and the off-diagonal ones from the chiral configurations.

An isolated dimer (7-Å distance between sites FCC and top) shows an antiferromagnetic isotropic exchange of 0.99 meV, and out-of-plane Dzialoshinskii-Moriya in-

teraction  $D_z = 0.11$  meV and an anisotropic symmetric exchange of  $J_s = 0.09$  meV. The collective effect of the adlayer leads to a reversal of the isotropic exchange interaction. Recent calculations [35] on Pb (110) show that the three terms of the exchange tensor that we just mention do present RKKY-like oscillations and can be of rather long range. Despite the small contribution of the anisotropic terms of the exchange tensor in our calculations, we cannot rule out a larger anisotropic contribution leading to chiral solutions of the spin texture for the adlayer.

### Spin wave Bloch theory

Bloch theory is a semiclassical approach (see for example the book by Yosida [36]) derived from the electromagnetic solution of an effective magnetic field obtained by fitting a mean-field approximation to the following



Hamiltonian:

$$\hat{H} = \sum_{i,j} J_{i,j} \vec{S}_i \cdot \vec{S}_j + \sum_i D_i S_{z,i}^2. \quad (2)$$

Where  $\vec{S}_i$  is the spin on site  $i$ ,  $J_{i,j}$  is the isotropic exchange interaction between spin on sites  $i$  and  $j$ ,  $D_i$  is the local longitudinal anisotropy on site  $i$  and  $S_{z,i}$  is the  $z$  component of the spin on site  $i$ . The assumption of the Bloch theory is a mean-field one where the spins follow the electromagnetic field created by the other spins and this gives rise to the Bloch equations.

For low-energy excitations, we can assume that spins change in only one unit. This is compatible with the spin-flips induced by a tunneling electron. Looking at the small variations with respect to the ground state (all spins aligned, ferromagnetic case) in the electromagnetic equations, the Bloch equations can be written like a harmonic oscillator of frequency  $\omega_q$ , where we assume already a 2-D spin array and wave vector  $q$ :

$$\hbar\omega_q = (D + J(0) - J(q))S, \quad (3)$$

where the Fourier transform of the exchange coupling is defined as

$$J(q) = \sum_{\vec{R}_j} J_{j,0} e^{-i\vec{q} \cdot \vec{R}_j}$$

with  $\vec{R}_j$  the lattice vector running over all the spin-array sites,  $j$ . These excitations are spinwaves that take into account the energy to flip a spin in the presence of the large molecular MAE,  $DS_z^2$ .

For the case of the Nc molecules, we take a simple RKKY interaction:

$$J(q) = \sum_j J_0 \cos(\vec{q} \cdot \vec{R}_j) \cos(2k_F R_j) / R_j^3, \quad (4)$$

where  $R_j$  is the modulus of the lattice vector  $\vec{R}_j$ . Both  $k_F$  and  $J_0$  are optimized to approximate the DFT values for the intra- and inter- dimer ferromagnetic exchange interactions. Neglecting the RKKY interaction and just taking a nearest-neighbor  $J$  leads to van Hove-like singularities in the excitation spectra that are not realistic.

### Simulation of differential conductance

Using the same approach of Refs. [29, 30], we assume that the current is proportional to the convolution of the tip's and sample's densities of states,  $\rho_T(\omega)$  and  $\rho_S(\omega)$ , respectively. Hence, the differential conductance is given by

$$\begin{aligned} \frac{\partial I}{\partial V} &\propto \int \rho_S(\omega) \frac{\partial \rho_T(\omega - eV)}{\partial V} [f(\omega - eV, T) - f(\omega, T)] d\omega \\ &+ \int \rho_S(\omega) \rho_T(\omega - eV) \frac{\partial f(\omega - eV, T)}{\partial V} d\omega \end{aligned} \quad (5)$$

For the tip, we assume a simple BCS density of states (DOS) with a phenomenological broadening Dynes parameter  $\gamma$  to broaden the quasiparticle singularities:

$$\rho_{BCS}(\omega) \propto \text{sgn}(\omega) \text{Re} \left( \frac{\omega + i\gamma}{\sqrt{(\omega + i\gamma)^2 - \Delta^2}} \right). \quad (6)$$

For the substrate,  $\rho_S(\omega)$  is computed using the spin-wave excitations, Eq. (3). The electronic density of states,  $\rho_S(\omega)$ , is the imaginary part of the propagator of an electron in the presence of spin excitations. The electron yields  $\hbar\omega_q$  every time it excites a spinwave. In order for this process to be possible, it needs to end up in an empty state of the BCS density of state. As a consequence, the electronic density of states in the presence of spin excitations is approximately:

$$\rho_S(\omega) = A\rho_{BCS}(\omega) + \sum_q \rho_{BCS}(\omega - \omega_q). \quad (7)$$

The first term is the elastic contribution, or the density of states without excitations. It is weighed by a parameter  $A$  to fit the ratio of elastic to inelastic contribution. The second term yields the contribution of each spinwave to the electronic density of states. Since the spinwaves are equivalent spin-flip excitations, we assume they enter with the same weight.

The calculations are performed using the experimental temperature, 2.5 K, and a gaussian broadening of 180  $\mu\text{eV}$  due to RF-noise and lock-in amplification in order to reproduce the experimental QP conductance. The same parameters were later used for the IETS peak.

---

\* Electronic address: deungjang.choi@ehu.eus

- [1] T.-P. Choy, J. M. Edge, A. R. Akhmerov, and C. W. J. Beenakker, *Physical Review B* **84**, 195442 (2011), URL <https://link.aps.org/doi/10.1103/PhysRevB.84.195442>.
- [2] F. Pientka, L. I. Glazman, and F. von Oppen, *Physical Review B* **88**, 155420 (2013), URL <http://link.aps.org/doi/10.1103/PhysRevB.88.155420>.
- [3] F. Pientka, Y. Peng, L. Glazman, and F. von Oppen, *Physica Scripta* **T164**, 014008 (2015).
- [4] S. Nadj-Perge, I. K. Drozdov, B. A. Bernevig, and A. Yazdani, *Physical Review B* **88** (2013), ISSN 1098-0121, 1550-235X, arXiv:1303.6363 [cond-mat], URL <http://arxiv.org/abs/1303.6363>.
- [5] S. Nadj-Perge, I. K. Drozdov, J. Li, H. Chen, S. Jeon, J. Seo, A. H. MacDonald, B. A. Bernevig, and A. Yazdani, *Science* p. 1259327 (2014), ISSN 0036-8075, 1095-9203, URL <http://science.sciencemag.org/content/early/2014/10/01/science.1259327>.
- [6] S. Jeon, Y. Xie, J. Li, Z. Wang, B. A. Bernevig, and A. Yazdani, *Science* **358**, 772 (2017), ISSN 0036-8075, 1095-9203, URL <http://science.sciencemag.org/content/358/6364/772>.

- [7] H. Kim, A. Palacio-Morales, T. Posske, L. Rzsá, K. Palots, L. Szunyogh, M. Thorwart, and R. Wiesendanger, *Science Advances* **4**, eaar5251 (2018), ISSN 2375-2548, URL <http://advances.sciencemag.org/content/4/5/eaar5251>.
- [8] A. Kamlapure, L. Cornils, J. Wiebe, and R. Wiesendanger, *Nature Communications* **9**, 3253 (2018), ISSN 2041-1723, URL <https://doi.org/10.1038/s41467-018-05701-8>.
- [9] A. Palacio-Morales, E. Mascot, S. Cocklin, H. Kim, S. Rachel, D. K. Morr, and R. Wiesendanger, *Science Advances* **5** (2019), URL <https://advances.sciencemag.org/content/5/7/eaav6600>.
- [10] J. Li, T. Neupert, Z. Wang, A. H. MacDonald, A. Yazdani, and B. A. Bernevig, *Nature Communications* **7**, 12297 (2016), ISSN 2041-1723, URL <https://www.nature.com/articles/ncomms12297>.
- [11] Z. Papi, R. S. Mong, A. Yazdani, and M. P. Zaletel, *Physical Review X* **8** (2018), ISSN 2160-3308, URL <https://link.aps.org/doi/10.1103/PhysRevX.8.011037>.
- [12] D.-J. Choi, N. Lorente, J. Wiebe, K. von Bergmann, A. F. Otte, and A. J. Heinrich, *Rev. Mod. Phys.* **91**, 041001 (2019), URL <https://link.aps.org/doi/10.1103/RevModPhys.91.041001>.
- [13] M. Ruby, F. Pientka, Y. Peng, F. von Oppen, B. W. Heinrich, and K. J. Franke, *Phys. Rev. Lett.* **115**, 197204 (2015), URL <https://link.aps.org/doi/10.1103/PhysRevLett.115.197204>.
- [14] K. J. Franke, G. Schulze, and J. I. Pascual, *Science* **332**, 940 (2011), ISSN 0036-8075, 1095-9203, URL <http://www.sciencemag.org/content/332/6032/940>.
- [15] N. Tsukahara, S. Shiraki, S. Itou, N. Ohta, N. Takagi, and M. Kawai, *Physical Review Letters* **106**, 187201 (2011), URL <http://link.aps.org/doi/10.1103/PhysRevLett.106.187201>.
- [16] Y. Jiang, Y. N. Zhang, J. X. Cao, R. Q. Wu, and W. Ho, *Science* **333**, 324 (2011), URL <http://www.sciencemag.org/content/333/6040/324.abstract>.
- [17] N. Hatter, B. W. Heinrich, M. Ruby, J. I. Pascual, and K. J. Franke, *Nature Communications* **6**, 8988 (2015), ISSN 2041-1723, URL <https://doi.org/10.1038/ncomms9988>.
- [18] N. Koci, D. Blank, P. Abufager, N. Lorente, S. Decurtins, S.-X. Liu, and J. Repp, *Nano Letters* **19**, 2750 (2019), pMID: 30933563, <https://doi.org/10.1021/acs.nanolett.8b03960>, URL <https://doi.org/10.1021/acs.nanolett.8b03960>.
- [19] G. Serrano, L. Poggini, M. Briganti, A. L. Sorrentino, G. Cucinotta, L. Malavolti, B. Cortigiani, E. Otero, P. Saintavit, S. Loth, et al., *Nature Materials* **19**, 546 (2020), ISSN 1476-4660, URL <https://doi.org/10.1038/s41563-020-0608-9>.
- [20] M. Ormaza, N. Bachellier, M. N. Faraggi, B. Verlhac, P. Abufager, P. Ohresser, L. Joly, M. Romeo, F. Scheurer, M.-L. Bocquet, et al., *Nano Lett.* **17**, 1877 (2017), URL <http://dx.doi.org/10.1021/acs.nanolett.6b05204>.
- [21] M. Ormaza, P. Abufager, B. Verlhac, N. Bachellier, M. L. Bocquet, N. Lorente, and L. Limot, *Nat. Commun.* **8**, 1974 (2017), URL <https://doi.org/10.1038/s41467-017-02151-6>.
- [22] B. Verlhac, N. Bachellier, L. Garnier, M. Ormaza, P. Abufager, R. Robles, M.-L. Bocquet, M. Ternes, N. Lorente, and L. Limot, *Science* **366**, 623 (2019), ISSN 0036-8075, 1095-9203, URL <https://science.sciencemag.org/content/366/6465/623>.
- [23] N. Bachellier, B. Verlhac, L. Garnier, J. Zaldivar, C. Rubio-Verdú, P. Abufager, M. Ormaza, D.-J. Choi, M.-L. Bocquet, J. I. Pascual, et al., *Nature Communications* **11**, 1619 (2020), ISSN 2041-1723, URL <https://doi.org/10.1038/s41467-020-15266-0>.
- [24] N. Bachellier, M. Ormaza, M. Faraggi, B. Verlhac, M. Vérot, T. Le Bahers, M.-L. Bocquet, and L. Limot, *Phys. Rev. B* **93**, 195403 (2016), URL <http://link.aps.org/doi/10.1103/PhysRevB.93.195403>.
- [25] Please refer to the Supplemental Material.
- [26] G. Webb, F. Marsiglio, and J. Hirsch, *Physica C: Superconductivity and its Applications* **514**, 17 (2015), ISSN 0921-4534, superconducting Materials: Conventional, Unconventional and Undetermined, URL <http://www.sciencedirect.com/science/article/pii/S0921453415000647>.
- [27] S. Rolf-Pissarczyk, J. A. J. Burgess, S. Yan, and S. Loth, *Phys. Rev. B* **94**, 224504 (2016), URL <https://link.aps.org/doi/10.1103/PhysRevB.94.224504>.
- [28] S.-H. Ji, T. Zhang, Y.-S. Fu, X. Chen, X.-C. Ma, J. Li, W.-H. Duan, J.-F. Jia, and Q.-K. Xue, *Phys. Rev. Lett.* **100**, 226801 (2008), URL <https://link.aps.org/doi/10.1103/PhysRevLett.100.226801>.
- [29] M. Ruby, F. Pientka, Y. Peng, F. von Oppen, B. W. Heinrich, and K. J. Franke, *Physical Review Letters* **115**, 087001 (2015), URL <http://link.aps.org/doi/10.1103/PhysRevLett.115.087001>.
- [30] D.-J. Choi, C. Rubio-Verd, J. de Bruijckere, M. M. Ugeda, N. Lorente, and J. I. Pascual, *Nature Communications* **8**, 15175 (2017), ISSN 2041-1723, URL <https://www.nature.com/articles/ncomms15175>.
- [31] S. Kezilebieke, R. Zitko, M. Dvorak, T. Ojanen, and P. Liljeroth, *Nano Letters* **19**, 4614 (2019), pMID: 31251066, <https://doi.org/10.1021/acs.nanolett.9b01583>, URL <https://doi.org/10.1021/acs.nanolett.9b01583>.
- [32] M. Ormaza, P. Abufager, N. Bachellier, R. Robles, M. Verot, T. Le Bahers, M.-L. Bocquet, N. Lorente, and L. Limot, *J. Phys. Chem. Lett.* **6**, 395 (2015), URL <http://dx.doi.org/10.1021/jz5026118>.
- [33] H. I. Li, K. J. Franke, J. I. Pascual, L. W. Bruch, and R. D. Diehl, *Phys. Rev. B* **80**, 085415 (2009), URL <https://link.aps.org/doi/10.1103/PhysRevB.80.085415>.
- [34] J. Bouaziz, M. dos Santos Dias, A. Ziane, M. Benakki, S. Blügel, and S. Lounis, *New. J. Phys.* **19**, 023010 (2017).
- [35] A. Rébola and A. M. Lobos, *Phys. Rev. B* **100**, 235412 (2019), URL <https://link.aps.org/doi/10.1103/PhysRevB.100.235412>.
- [36] K. Yosida, *Theory of Magnetism*, Springer Series in Solid-State Sciences (Springer Berlin Heidelberg, 2010), ISBN 9783642082313, URL <https://books.google.es/books?id=56CBcgAACAAJ>.
- [37] B. W. Heinrich, J. I. Pascual, and K. J. Franke, *Progress in Surface Science* **93**, 1 (2018), ISSN 0079-6816, URL <http://www.sciencedirect.com/science/article/pii/S0079681618300017>.
- [38] L. Farinacci, G. Ahmadi, G. Reecht, M. Ruby, N. Bogdanoff, O. Peters, B. W. Heinrich, F. von Oppen, and K. J. Franke, *Phys. Rev. Lett.* **121**, 196803 (2018), URL <https://link.aps.org/doi/10.1103/PhysRevLett.121.196803>.

- [39] L. Malavolti, M. Briganti, M. Hänze, G. Serrano, I. Cimatti, G. McMurtrie, E. Otero, P. Ohresser, F. Totti, M. Mannini, et al., *Nano Letters* **18**, 7955 (2018), pMID: 30452271, <https://doi.org/10.1021/acs.nanolett.8b03921>, URL <https://doi.org/10.1021/acs.nanolett.8b03921>.
- [40] G. Kresse and J. Furthmüller, *Phys. Rev. B* **54**, 11169 (1996).
- [41] G. Kresse and D. Joubert, *Phys. Rev. B* **59**, 1758 (1999).
- [42] J. P. Perdew, K. Burke, and M. Ernzerhof, *Phys. Rev. Lett.* **77**, 3865 (1996), URL <https://link.aps.org/doi/10.1103/PhysRevLett.77.3865>.
- [43] S. Grimme, J. Antony, S. Ehrlich, and H. Krieg, *The Journal of Chemical Physics* **132**, 154104 (2010), URL <https://doi.org/10.1063/1.3382344>.
- [44] S. Grimme, S. Ehrlich, and L. Goerigk, *Journal of Computational Chemistry* **32**, 1456 (2011), URL <https://onlinelibrary.wiley.com/doi/abs/10.1002/jcc.21759>.
- [45] J. Tersoff and D. R. Hamann, *Physical Review Letters* **50**, 1998 (1983), URL <http://link.aps.org/doi/10.1103/PhysRevLett.50.1998>.
- [46] M.-L. Bocquet, H. Lesnard, S. Monturet, and N. Lorente, in *Computational Methods in Catalysis and Materials Science*, edited by R. A. v. Santen and P. Sautet (Wiley-VCH Verlag GmbH & Co. KGaA, 2009), pp. 199–219, ISBN 978-3-527-62548-2, URL <http://onlinelibrary.wiley.com/doi/10.1002/9783527625482.ch11/summary>.
- [47] N. Lorente and R. Robles, *STMpw* (2019), URL <https://zenodo.org/record/3581159>.
- [48] D.-J. Choi, R. Robles, S. Yan, J. A. J. Burgess, S. Rolf-Pissarczyk, J.-P. Gauyacq, N. Lorente, M. Ternes, and S. Loth, *Nano Letters* **17**, 6203 (2017), pMID: 28872317, <https://doi.org/10.1021/acs.nanolett.7b02882>, URL <https://doi.org/10.1021/acs.nanolett.7b02882>.
- [49] S. K. Panda, I. Di Marco, O. Grånäs, O. Eriksson, and J. Fransson, *Phys. Rev. B* **93**, 140101 (2016), URL <https://link.aps.org/doi/10.1103/PhysRevB.93.140101>.
- [50] A. B. Shick, F. Máca, and A. I. Lichtenstein, *Phys. Rev. B* **79**, 172409 (2009), URL <http://link.aps.org/doi/10.1103/PhysRevB.79.172409>.